Quantum computing critical exponents

Henrik Dreyer[1,2] Mircea Bejan[1] and Etienne Granet[1]

[1]*Rudolf Peierls Centre for Theoretical Physics, Clarendon Laboratory, Oxford OX1 3PU, United Kingdom*
[2]*Cambridge Quantum Computing Ltd., 9a Bridge Street, CB2 1UB Cambridge, United Kingdom*

We show that the variational quantum-classical simulation algorithm admits a finite circuit depth scaling collapse when targeting the critical point of the transverse field Ising chain. The order parameter only collapses on one side of the transition due to a slowdown of the quantum algorithm when crossing the phase transition. In order to assess performance of the quantum algorithm and compute correlations in a system of up to 752 qubits, we use techniques from integrability to derive closed-form analytical expressions for expectation values with respect to the output of the quantum circuit. We also reduce a conjecture made by Ho and Hsieh [W. W. Ho and T. H. Hsieh, SciPost Phys. **6**, 029 (2019)] about the exact preparation of the transverse field Ising ground state to a system of equations.

I. INTRODUCTION

Impressive advances have recently led to the realization of the first noisy intermediate-scale quantum (NISQ) computers [1–3] and quantum simulators [4–10]. One promising application of NISQ devices is the simulation of quantum many-body systems [6,11–16]. Near-term quantum computers will be limited by the number of qubits and the number of gates that can be executed with high fidelity, while analog simulations have to be executed within a typically short coherence time. These restrictions make it challenging to map out phase diagrams of strongly correlated materials, in particular in the vicinity of quantum critical points. At these phase transitions, the correlation length diverges and representing the system of interest with a finite device necessarily comes with a loss of accuracy. Instead of pushing computational resources towards the thermodynamic limit, classical methods typically make use of data produced by smaller-scale computations and combine those data points in an informed manner, as it is done in finite-size [17–20] or finite-bond-dimension scaling collapses [21].

Similarly, one may ask if data produced by a NISQ quantum computer can be used to predict the location and universality class of a critical point with an accuracy that goes beyond the machine specifications. In this work, we provide an example where this is indeed possible. More precisely, we show that the variational quantum classical simulation (VQCS) [22] algorithm admits a scaling collapse when targeting the critical point of the transverse field Ising model (TFIM). Instead of finite size or finite entanglement, the depth of the quantum circuit plays the role of the relevant perturbation away from criticality. To classically benchmark the performance of the quantum algorithm, we adapt techniques from integrability to the quantum computation setting. Specifically, the quantum circuit can be mapped to a sequence of quenches in the TFIM. We show how to describe the state

after a series of such quenches and derive a closed-form analytical expression for expectation values of local Gaussian observables (like the energy) in a circuit of arbitrary depth and width. This allows us to optimize the parameters of the quantum circuit for a number of qubits that is inaccessible to other classical simulation techniques but within reach of a NISQ computer.

Importantly, assessing the physics of the optimal state requires the evaluation of expectation values that are non-Gaussian or nonlocal. Our key technical contribution is a framework in which *arbitrary* observables can be evaluated classically in polynomial time, provided the circuit is Gaussian. Using this framework, we compute the order parameter of the optimal circuit. We find that finite-circuit-depth data of the order parameter collapses on one side of the phase transition, in the phase that contains the initial state of the quantum computer. The framework we develop can also be used as a point of departure for quantum circuit design and to benchmark quantum devices.

II. MODEL, ALGORITHM, AND METHOD

A. The VQCS algorithm

We study the VQCS algorithm that was put forward in [22] as an adaptation of the quantum approximate optimization algorithm (QAOA) [23,24] to quantum simulators. Generally, the strategy is to split a target Hamiltonian acting on L qubits as

$$H_T(h) = H_1 + hH_2, \quad (1)$$

where the ground state of H_1, $|\psi_1\rangle$, should be easy to initialize on a quantum computer or simulator. The VQCS ansatz consists in choosing a circuit depth $2p$ as well as $2p$ variational parameters $(\gamma_1, \beta_1, \ldots, \gamma_p, \beta_p)$ and writing

$$|\psi(\gamma, \beta)\rangle = e^{-i\beta_p H_1} e^{-i\gamma_p H_2} \cdots e^{-i\beta_1 H_1} e^{-i\gamma_1 H_2} |\psi_1\rangle. \quad (2)$$

We take the cost function to be the energy density

$$F_L(h; \gamma, \beta) = \frac{1}{L} \langle \psi(\gamma, \beta)|H_T(h)|\psi(\gamma, \beta)\rangle, \qquad (3)$$

where we have made explicit L, the number of qubits that $H_T(h)$ acts on. The VQCS algorithm proceeds by measuring the cost function on the quantum computer or simulator and feeding the input to an optimization routine running on a classical computer. Once the optimal value

$$F_L(h; p) = \min_{\gamma, \beta} F_L(h; \gamma, \beta) \qquad (4)$$

is found, the corresponding quantum states can be prepared at will using the optimal parameters $(\gamma_{\text{opt}}, \beta_{\text{opt}})$ and observables of interest can be measured.

B. Transverse field Ising model

In this paper, we choose as the target Hamiltonian the TFIM

$$H_1 = -\sum_{i=1}^{L} Z_i Z_{i+1}, \qquad (5)$$

$$H_2 = -\sum_{i=1}^{L} X_i, \qquad (6)$$

where $X = \begin{pmatrix} 0 & 1 \\ 1 & 0 \end{pmatrix}$ and $Z = \begin{pmatrix} 1 & 0 \\ 0 & -1 \end{pmatrix}$ and where periodic boundary conditions are imposed. To be precise, H_1 has two ground states and we pick $|\psi_1\rangle = |0 \dots 0\rangle$ with $Z|0\rangle = +|0\rangle$ to initialize the algorithm. The fact that H_1 and H_2 consist of local commuting terms has two consequences: (i) The evolution (2) can be implemented on a digital quantum computer without Trotterization and (ii) we can simulate the algorithm directly in the thermodynamic limit. More precisely,

$$F_L(h; \gamma, \beta) = F_{L'}(h; \gamma, \beta) \qquad (7)$$

for $L, L' \geqslant 4p$. This is due to the fact that there is an exact finite light cone for local operators, as illustrated in Fig. 1. In the regime $L \geqslant 4p$ the boundary conditions also become irrelevant. Therefore, for a given p, a quantum computer with $L = 4p$ qubits captures the thermodynamic limit exactly and this is the setting we will later choose in our simulation.[1]

Besides the energy, we are also interested in the scaling behavior of the observables

$$m_Z(h; p) = \langle \psi(\gamma_{\text{opt}}, \beta_{\text{opt}})|Z_j|\psi(\gamma_{\text{opt}}, \beta_{\text{opt}})\rangle, \qquad (8)$$

$$m_X(h; p) = \langle \psi(\gamma_{\text{opt}}, \beta_{\text{opt}})|X_j|\psi(\gamma_{\text{opt}}, \beta_{\text{opt}})\rangle, \qquad (9)$$

$$m_{XX}(\ell; h; p) = \langle \psi(\gamma_{\text{opt}}, \beta_{\text{opt}})|X_j X_{j+\ell}|\psi(\gamma_{\text{opt}}, \beta_{\text{opt}})\rangle \\ - m_X(h; p)^2, \qquad (10)$$

where the position j is arbitrary due to translation invariance of both the initial state and the circuit.

———————

[1]Empirically, we find that $L, L' \geqslant 2p + 2$ is sufficient for (7) to hold.
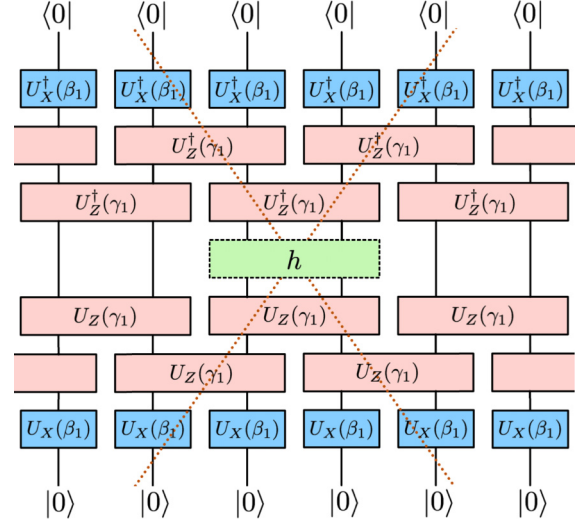

FIG. 1. Quantum circuit (2) for $p = 1$. The expectation value of the energy density h involves only those qubits that are within the light cone (dotted). Here $U_X(\beta) = \exp(i\beta X)$ and $U_{ZZ}(\gamma) = \exp(i\gamma Z \otimes Z)$. A similar circuit provides the gradient

C. Exact solution of the quantum circuit

General techniques suffer from a cost per optimization step that is exponential in the system size, limiting the availability of data to $L \lesssim 20$. To study the fate of the algorithm closer towards the scaling limit, we turn to techniques from integrability. As we show in Appendix A, the energy F, magnetization m, and overlap ϕ of $|\psi(\gamma, \beta)\rangle$ with the exact ground state of the target Hamiltonian admit closed-form expressions.

In order to present these results, let us introduce the sequence of functions $f_j(k)$ for $j = 0, \dots, 2p$ that satisfy the recurrence relation

$$f_0(k) = 0,$$

$$f_{2j+1}(k) = e^{-4i\gamma_{j+1}} \frac{1 - i\tan(k/2)f_{2j}(k)}{f_{2j}(k) - i\tan(k/2)}, \qquad (11)$$

$$f_{2j}(k) = e^{-4i\beta_j} \frac{1 + i\tan(k/2)f_{2j-1}(k)}{f_{2j-1}(k) + i\tan(k/2)}.$$

We then define

$$f_{\text{proj}}(k) = \frac{iK_{h0}(k) + f_{2p}(k)}{1 + iK_{h0}(k)f_{2p}(k)},$$

$$\text{with } K_{h0}(k) = \tan \frac{1}{2} \left[\arctan \frac{h - \cos k}{\sin k} \right.$$

$$\left. + \arctan \frac{1}{\tan k} \right],$$

$$\varepsilon_h(k) = \begin{cases} 2\sqrt{1 + h^2 - 2h\cos k}, & k \neq 0 \\ -2(1 - h), & k = 0, \end{cases} \qquad (12)$$

as well as the sets

$$\text{NS} = \left\{ \frac{2\pi(n+1/2)}{L}, n = -L/2, \ldots, L/2-1 \right\},$$

$$\text{R} = \left\{ \frac{2\pi n}{L}, n = -L/2, \ldots, L/2-1 \right\}, \tag{13}$$

and $\text{NS}_+, \text{R}_+ \subset \text{NS}, \text{R}$ the subsets of strictly positive elements. Then the energy density $F_L(h; \gamma, \beta)$ of the state $|\psi(\gamma, \beta)\rangle$ is

$$F_L(h; \gamma, \beta) = \frac{1}{2L} \sum_{k \in \text{NS} \cup \text{R}} \varepsilon_h(k) \frac{|f_{\text{proj}}(k)|^2}{1 + |f_{\text{proj}}(k)|^2}$$

$$- \frac{1}{4L} \sum_{k \in \text{NS} \cup \text{R}} \varepsilon_h(k). \tag{14}$$

This expression for the energy density holds in arbitrary finite-size L. As for the overlap with the ground state, an exact formula is given in Appendix A.

In the thermodynamic limit $L \to \infty$, the X magnetization is given by

$$m_X(h; p) = 1 - \frac{1}{\pi} \int_{-\pi}^{\pi} \frac{|g_{2p}(k)|^2}{1 + |g_{2p}(k)|^2} dk, \tag{15}$$

with

$$g_{2p}(k) = \frac{1 - i \tan(k/2) f_{2p}(k)}{f_{2p}(k) - i \tan(k/2)}. \tag{16}$$

The connected XX-magnetization correlation is given by

$$m_{XX}(\ell; h; p) = \left| \frac{1}{\pi} \int_{-\pi}^{\pi} \frac{g_{2p}(k) e^{-ik\ell}}{1 + |g_{2p}(k)|^2} \right|^2$$

$$- \left| \frac{1}{\pi} \int_{-\pi}^{\pi} \frac{|g_{2p}(k)|^2 e^{-ik\ell}}{1 + |g_{2p}(k)|^2} \right|^2. \tag{17}$$

The Z magnetization is expressed as a Fredholm determinant

$$m_Z(h; p) = \det(\text{Id} - J). \tag{18}$$

Here $J(\lambda, \mu)$ is the function defined on $[0, \pi] \times [0, \pi]$,

$$J(\lambda, \mu) = \frac{2}{\pi} \frac{\rho(\lambda) \sin \lambda}{f_{2p}(\lambda)} \frac{1}{\cos \lambda - \cos \mu}$$

$$\times \left[\fint_0^{\pi} \frac{f_{2p}(k) \sin k}{\cos \lambda - \cos k} dk - \fint_0^{\pi} \frac{f_{2p}(k) \sin k}{\cos \mu - \cos k} dk \right], \tag{19}$$

where $\fint$ denotes an integral in principal value and

$$\rho(k) = \frac{1}{2\pi} \frac{|f_{2p}(k)|^2}{1 + |f_{2p}(k)|^2}. \tag{20}$$

Finally, if the algorithm is initialized in $|+ \cdots +\rangle$ with $X |+\rangle = |+\rangle$, then the relations (11)–(17) hold true with $f_0(k) = \frac{1}{i \tan(k/2)}$ in (11) and with (14) multiplied by 2 and summation only in NS. Crucially, all of these quantities can be computed in time and memory that scale as polynomials in p. Equations (11)–(20) are the central result of this paper.

A few comments are in order. First, as shown in Appendix B, one can generalize the exact solution to allow for rounds of $\exp(it \sum_{j=1}^{L} Y_j Y_{j+1})$ gates in the quantum circuit
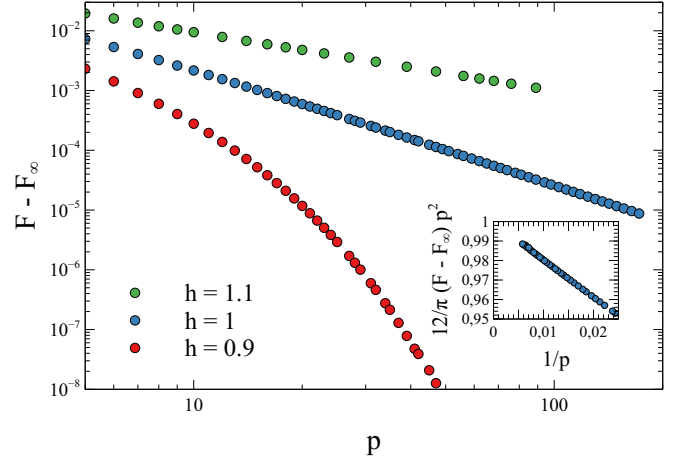

FIG. 2. Difference between the optimal energy density in the thermodynamic limit $F_L(h; \gamma, \beta)$ after p steps and the exact ground-state value, as a function of p, for $h = 1$ (middle blue circles), $h = 0.9$ (lower red circles), and $h = 1.1$ (upper green circles). The inset shows the behavior $\frac{\pi}{12p^2}$ for $h = 1$.

(2). Second, in the case where the algorithm is initialized in $|+ \cdots +\rangle$, it was conjectured in [22] that the ground state in finite-size L can be exactly prepared with $p = L/2$ steps. In our formalism, this conjecture translates to the statement that, for $f_0(k) = \frac{1}{i \tan(k/2)}$, the system of $L/2$ equations $f_{\text{proj}}(k) = 0$, $k \in \text{NS}_+$, for L real unknowns $\gamma_1, \beta_1, \ldots, \gamma_p, \beta_p$ admits at least one solution. Third, as explained in Appendix C, as a by-product of our calculations we obtain the solution to the long-standing problem of the full time evolution of the order parameter after a quantum quench in the Ising model [25–38]. Fourth, while we focus on the ground state in the main text, it is possible to target excited states using a variant of (A28). Finally, to find the optimal solution, we use a Broyden-Fletcher-Goldfarb-Shanno algorithm, supplying the gradient of (14), for which an analytic formula is available.

III. RESULTS

All of the following results are given for the effective thermodynamic limit $L = 4p$.

A. Energy

The optimal parameters γ, β are fed into (14) to obtain the energy of the lowest-energy state that can be prepared with the quantum computer after p steps. The energy density is then compared to the known value in the thermodynamic limit,

$$F_\infty(h) = -\frac{1}{2\pi} \int_0^{\pi} \varepsilon_h(k) dk. \tag{21}$$

The results are plotted in Fig. 2 for three different values of the magnetic field $h = 1$, $h < 1$, and $h > 1$. We observe the leading behavior

$$F_L(h; \gamma, \beta) - F_\infty(h) = \begin{cases} A e^{-\lambda p} & \text{if } h < 1 \\ \frac{\pi}{12p^2} & \text{if } h = 1 \\ \frac{B}{p} & \text{if } h > 1, \end{cases} \tag{22}$$
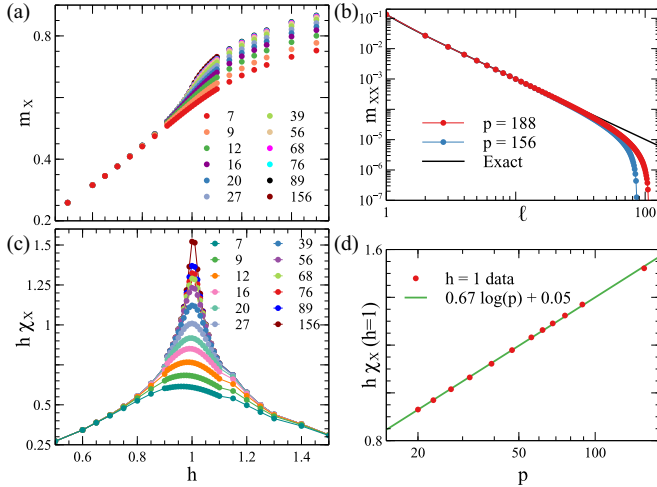
FIG. 3. (a) Magnetization in the X direction at the optimal angles at circuit depth p as a function of h. Larger values correspond to larger circuit depths. (b) Connected correlation of the magnetization in the X as a function of ℓ for optimal angles at $h = 1$. The line curving down at larger ℓ corresponds to $p = 188$. (c) Susceptibility in the X direction at the optimal angles at circuit depth p as a function of h. Larger values correspond to larger circuit depths. (d) Logarithmic divergence of the susceptibility at $h = 1$. The logarithm is with respect to base 10. The lines guide the eye.

with A, B, λ some h-dependent constants. The factor $\frac{\pi}{12}$ is observed with precision $\sim 10^{-5}$. For $h \gg 1$, if we rescale the Hamiltonian by a factor $1/h$, the constant B reaches a finite value.

We recall that the energy density of the exact ground state in finite-size L would converge to its value in the thermodynamic limit exponentially fast for $h \neq 1$, while at $h = 1$ the energy difference would have the leading behavior $-\frac{\pi v_F c}{6L^2}$ with $v_F = 2$ the Fermi velocity and $c = \frac{1}{2}$ the central charge of the conformal field theory describing the critical point [39–41]. We remark that for $h \leqslant 1$ the behavior (22) is qualitatively the same in terms of the circuit depth p. In particular, the behavior at the critical point could suggest a general leading-order correction of $\frac{\pi v_F c}{12p^2}$.

However, for $h > 1$ we observe a slowdown of the algorithm that bears similarities with adiabatic slowdown near criticality [42]: Adiabatically evolving across a critical point typically requires time $\sim 1/\Delta^2$ if Δ is the smallest gap of the system. Since the quantum computer is initialized in the symmetry-broken phase of the Ising model and the circuit respects the symmetry, a slowdown when targeting $h > 1$ is expected. Conversely, when we initialize the computation in the paramagnetic $|+ \cdots +\rangle$ state, the reverse scaling (22) is observed: The energy density converges exponentially fast for $h > 1$, as $\frac{\pi}{12p^2}$ for $h = 1$ and is proportional to $1/p$ for $h < 1$.

B. The X magnetization

We plot in Fig. 3 the expectation value $m_X(h; p)$ of the X magnetization and its susceptibility $\chi_X(h; p) = \partial_h m_X(h; p)$ at optimal parameters (γ, β) at circuit depth p, as a function of h. We observe a logarithmic divergence $\frac{2}{\pi} \log p$ of $\chi_X(h; p)$ at $h = 1$, signaling a phase transition. The susceptibility is
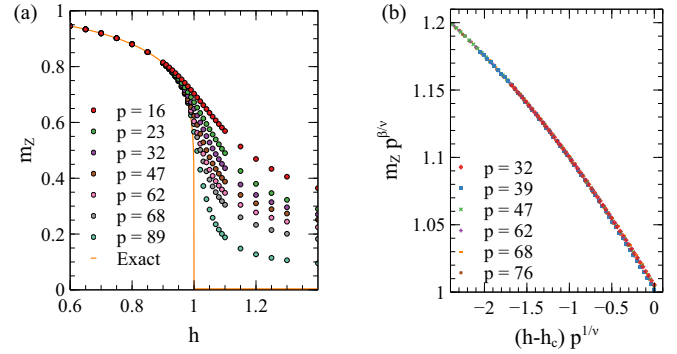

FIG. 4. (a) Magnetization in the Z direction at the optimal angles at circuit depth p as a function of h. Larger circuit depth corresponds to smaller m_Z. (b) One-sided collapse of the magnetization curves for 50 linearly spaced points between $h = 0.95$ and $h = 1$, using the optimized exponents (see the text).

indeed known to diverge at the critical point with critical exponent $\alpha = 0$ [43].

We also show in Fig. 3 the expectation value $m_{XX}(\ell; h; p)$ of the connected XX-magnetization correlation at the critical point $h = 1$, as a function of the distance ℓ. The exact known value is $m_{XX}^{\text{exact}}(\ell) = \frac{4}{\pi^2} \frac{1}{4\ell^2 - 1}$ [44]. With a circuit depth $p = 188$, this exact value is well reproduced for $\ell \lesssim 20$ and the critical exponent 2 is observed up to $\ell \approx 30$. Our data for various values of p suggest that the correlation length, defined as the minimum distance ℓ for which $m_{XX}(\ell)/m_{XX}^{\text{exact}} < 1/e$, scales linearly as $0.44p$. We remark that while being proportional to the effective system size $L = 4p$, this correlation length is smaller than the effective correlation length of the finite-size ground state which we have computed to behave as $0.44L$. This suggests that it is difficult to create long-range correlations with a VQCS or QAOA-like algorithm.

C. The Z magnetization and finite-circuit-depth scaling

We now discuss the scaling of the order parameter, $m_Z(h; p)$. The exact value in the thermodynamic limit is known to be $(1 - h^2)^{1/8}$ for $h \leqslant 1$ and 0 for $h > 1$ [44]. The behavior of $m_Z(h; p)$ at optimal parameters (γ, β), as shown in Fig. 4, is qualitatively similar to the ground-state magnetization in finite-size L due to the finite light cone introducing a length scale less than or equal to $4p$. As we have observed in the preceding section, the correlation length $\xi(p)$ of the optimal states at circuit depth p is significantly smaller. Nevertheless, since ξ is linear in p, we expect the convergence in p and ξ to be characterized by the same exponents.

If the circuit reproduces the finite-size ground state sufficiently well, one may estimate the critical exponents by directly adapting finite-size arguments to obtain a scaling hypothesis for finite *circuit depth* scaling: Denoting by ν the critical exponent associated with the divergence of the correlation length $\xi \sim |h - h_c|^{-\nu}$ close to the critical point h_c and by β the critical exponent of the Z magnetization $m_Z(h; p) \sim |h - h_c|^\beta$, there exists a scaling function φ such that for large p and h close to h_c,

$$m_Z(h; p) p^{\beta/\nu} = \varphi((h - h_c) p^{1/\nu}). \tag{23}$$

There is however an important difference with finite-size scaling. We observed in Sec. III A that the convergence of the energy density as a function of p is qualitatively similar to that in finite-size L for $h < h_c$ and $h = h_c$ only. For $h > h_c$ the quantum circuit retains knowledge of the initial state and the behavior in terms of the circuit depth significantly differs. As a consequence, one should generally expect finite-circuit-depth scaling to follow finite-size scaling only before the critical point. Having established $h_c = 1$ from the X susceptibility, optimizing the collapse using pyfssa [45] yields $\beta = 0.122$ and $\nu = 0.99$, in good agreement with the known values $\beta_{exact} = 0.125$ and $\nu_{exact} = 1$, and such a one-sided collapse is indeed observed for those values (see Fig. 4).

D. Structure of the optimal solutions

A key performance metric for variational quantum algorithms is the structure of the resulting energy landscape: An algorithm can only yield exponential speedup if the classical optimizer does not need to call the quantum subroutine too often and if local minima can be avoided. In this section we describe the structure of the solutions (γ, β) that minimize the energy density in the thermodynamic limit at fixed p. We note that one can always add a multiple of $\pi/2$ to any of the angles without changing the state, so one can choose that they lie in $[0, \pi/2[$. We observe that for a circuit depth p, there are 2^p different sets of optimal angles (γ, β) that yield exactly the same energy density in the thermodynamic limit $L \geqslant 4p$. This structure has been checked for $p \leqslant 5$, and we conjecture that it holds true for all p. One half of those minima are accounted for by the invariance of the energy under mapping $\gamma_j \rightarrow \pi/2 - \gamma_j$ and $\beta_j \rightarrow \pi/2 - \beta_j$ for all j, as can be seen by direct inspection of (14). Characterizing the remaining solutions is the goal of the remainder of this section.

Empirically, we find that the expectation values of the X magnetization and the mode occupation numbers are identical in all of the "branches." In particular, the absolute value $|f_{proj}(k)|$ is branch independent. These observables share a common trait: After a Jordan-Wigner mapping from the spin to fermionic degrees of freedom (cf. Appendix A), they correspond to quadratic fermion operators. Other observables such as the Z-magnetization or the XX-magnetization correlations vary among the different branches (cf. Fig. 5). In particular, the phase of $f_{proj}(k)$ depends on the branch. This branch dependence translates into the fact that at fixed finite p, the optimal energy for the TFIM Hamiltonian coupled to the observable of study would be discontinuous at vanishing coupling parameter.

For $h < 1$, the distributions of expectation values become more and more peaked for $p \rightarrow \infty$ and converge to the same value among the different branches, reflecting the fact that all solutions converge to the same state. However, for $h > 1$, our data suggest that this convergence could depend on the observable. While this convergence is observed to hold for the XX-magnetization correlation, our numerics suggest that, for $h > 1$, the different branches could have different Z magnetization even in the $p \rightarrow \infty$ limit.

To summarize this section, the energy landscape produced by the quantum circuit at depth p is exponentially
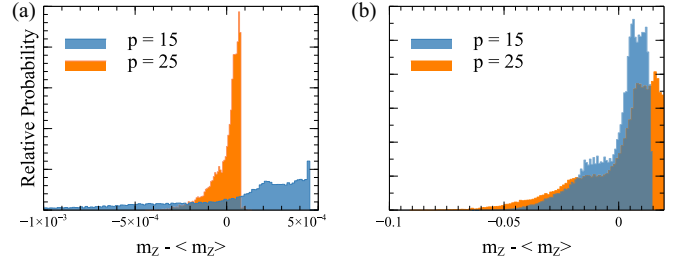

FIG. 5. Histogram of the Z magnetization m_Z of the optima obtained from 250 000 (80 000) random initializations of the optimization for $p = 15$ ($p = 25$) and targets (a) $h = 0.9$ and (b) $h = 1.1$. The higher peak corresponds to $p = 25$ in (a) and to $p = 15$ in (b). The angles are each initialized uniformly at random in $[0, \pi/2]$. The average over all samples is denoted by $\langle m_Z \rangle$. For $h = 0.9$, m_Z converges to the ground-state magnetization, while, across the phase transition at $h = 1.1$, such convergence is not observed for $p \leqslant 25$.

degenerate. Apart from some observables that are quadratic in the fermions, generic observables differ between different optima. If the target Hamiltonian is in the same phase as the initial state, these expectation values converge to the ground-state expectation value.

E. Preparation time

An attractive property of the VQCS algorithm is the fact that it is amenable to analog quantum simulation. In this case, the parameters (γ, β) are interpreted as real times and the main criterion for the feasibility of the algorithm is the total time

$$T(p) = \sum_{j=1}^{p} \gamma_{opt}^j + \sum_{j=1}^{p} \beta_{opt}^j, \tag{24}$$

where all γ_{opt}^j and β_{opt}^j are assumed to be in $[0, \pi/2[$. If $T(p) \propto p$, then the same scaling relation (23) holds, with p replaced by T. Since the optimal solution is not unique (cf. Sec. III D), we take $T(p)$ to be the average total time over different branches. Numerically, we find that, on average, $\langle \beta_{opt}^j \rangle, \langle \gamma_{opt}^j \rangle \sim \pi/4$ such that $T(p) \sim \frac{\pi}{2} p$. This is maximal in the sense that for every solution with $T(p) > \frac{\pi}{2} p$, there exists a solution with $T'(p) = \pi p - T(p) < \frac{\pi}{2} p$, and so one can impose $T(p) \leqslant \frac{\pi}{2} p$.

IV. DISCUSSION AND OUTLOOK

We have shown that data obtained from small-scale quantum computers or simulators can be used in an informed way to accurately estimate the location and universality class of a quantum critical point. To this end, we have taken the perspective of quantum computation as a series of quenches and used techniques from integrability to obtain closed-form expressions for the output of the VQCS algorithm. These methods exceptionally allowed us to reach the quantum regime of the VQCS and QAOA algorithms, otherwise inaccessible to classical simulations and as of today still difficult to access with actual quantum computers. The existence of this *exact solution* to QAOA opens invaluable possibilities of testing and

benchmarking the algorithm, as well as of gaining intuition about its output such as the angles γ and β.

While these methods were necessary to argue about computations with more than ∼20 qubits, they raise the question if similar scaling behavior extends to nonintegrable target Hamiltonians. We stress that the outcome of the quantum circuit is classically tractable independent of the target Hamiltonian, as long as the circuit is Gaussian. In this context, especially $2 + 1D$ quantum critical points would be interesting to investigate since a number of both digital and analog quantum devices naturally realize a two-dimensional architecture, while conformal data are hard to come by.

Regarding the slowdown of the algorithm across the phase transition, one may allow the circuit to break the symmetry of the target Hamiltonian, including gates like $\exp(i\delta Z)$. This may allow the computation to circumvent the critical point, potentially improving the scaling collapse (23).

Naturally, circuits providing quantum advantage on NISQ devices will not be Gaussian and designing such circuits is a major challenge. The energy landscape may be sufficiently hostile that a random initialization and optimization procedure is bound to fail; instead, usual contemporary approaches include only a small number of parameters relying on physical insight like the adiabatic theorem, coupled-cluster wave functions, imaginary-time evolution, or dynamical mean-field theory [46–66]. Adding a new, classically tractable ansatz to the toolkit may provide another useful starting point for quantum circuit design.

We also mention that, for large p, VQCS can mimic adiabatic evolution, yet the optimal evolution times we find at large p do not generally bear the structure of Trotterized adiabatic time evolution. Our techniques could be adapted to study the behavior of quasiadiabatic trajectories in the large-p limit more generally.

Furthermore, it would be interesting to investigate the fate of this particular algorithm under noise. In the presence of an exponentially degenerate optimization landscape, small inaccuracies may even be beneficial by lifting degeneracies, while the linear depth of the algorithm circumvents an exponential slowdown due to noise-induced barren plateaus [67]. We leave these questions to future work.

APPENDIX A: THE X AND ZZ GATES

1. Solution of the TFIM

We first recall a number of results on the diagonalization of the TFIM that can be found in Appendix A of [29] and that we briefly summarize here for self-completeness. The TFIM is defined as

$$H(h) = -\sum_{j=1}^{L} Z_j Z_{j+1} + h X_j, \quad \text{(A1)}$$

with periodic boundary conditions. It is diagonalized by performing a Jordan-Wigner transformation on the spin operators into fermions $\{c_j, c_l^\dagger\} = \delta_{jl}$,

$$X_j = 1 - 2c_j^\dagger c_j, \quad Z_j = (c_j + c_j^\dagger) \prod_{l=1}^{j-1} (1 - 2c_l^\dagger c_l), \quad \text{(A2)}$$

followed by a Bogoliubov transformation of the Fourier modes

$$c(k) = \frac{1}{\sqrt{L}} \sum_{j=1}^{L} e^{ijk} c_j \quad \text{(A3)}$$

into fermionic operators $\{\alpha_{h;j}, \alpha_{h;l}^\dagger\} = \delta_{jl}$,

$$c(k) = \cos \frac{\theta_k^h}{2} \alpha_{h;k} + i \sin \frac{\theta_k^h}{2} \alpha_{h;-k}^\dagger,$$

$$c^\dagger(k) = -i \sin \frac{\theta_k^h}{2} \alpha_{h;-k} + \cos \frac{\theta_k^h}{2} \alpha_{h;k}^\dagger, \quad \text{(A4)}$$

where θ_k^h is defined by

$$e^{i\theta_k^h} = \frac{h - e^{ik}}{\sqrt{1 + h^2 - 2h \cos k}}. \quad \text{(A5)}$$

The Hamiltonian conserves the parity of $\hat{N} = \sum_{j=1}^{L} c_j^\dagger c_j$ and so splits into two sectors, called Neveu-Schwarz (NS) and Ramond (R). If $\hat{N}$ is even the momentum k in (A3) takes values in NS, while if $\hat{N}$ is odd it takes values in R, both sets being defined in (13). Denoting by $|0\rangle_h^{R,NS}$ the vacuum state in these two sectors, the eigenstates of $H(h)$ then read, for $k \subset NS$ or $k \subset R$,

$$|k\rangle_h \equiv \alpha_{h;k_1}^\dagger \cdots \alpha_{h;k_m}^\dagger |0\rangle_h^{R,NS}, \quad \text{(A6)}$$

with m even in the NS sector and odd in the R sector. The Hamiltonian $H(h)$ is then expressed as

$$H(h) = \sum_{k \in NS} \varepsilon_h(k) \alpha_{h;k}^\dagger \alpha_{h;k}$$
$$+ \sum_{k \in R} \varepsilon_h(k) \alpha_{h;k}^\dagger \alpha_{h;k} - \frac{1}{2} \sum_{k \in NS,R} \varepsilon_h(k), \quad \text{(A7)}$$

with $\varepsilon_h(k)$ defined in (12) and where the last sum of this expression is performed on NS or R according to the sector of the states on which the Hamiltonian is applied.

For $h > 1$ the ground state is $|0\rangle_h^{NS}$. For $h < 1$ the two lowest-energy levels are $|0\rangle_h^{NS}$ and $\alpha_{h;0}^\dagger |0\rangle_h^R$ and their energy difference is exponentially small in the system size L. At $h = 0$, the ground state is exactly twofold degenerate and its corresponding eigenspace is generated by $|0\rangle^{\otimes L}$ and $|1\rangle^{\otimes L}$, with $|0\rangle$ and $|1\rangle$ the two eigenvectors of Z with eigenvalues 1 and -1. Their sum is in NS and so is proportional to $|0\rangle_0^{NS}$; their difference is in R and so is proportional to $\alpha_{0;0}^\dagger |0\rangle_0^R$. Hence one can choose the arbitrary phase of the vacuum states so that the state $|\psi_1\rangle$ introduced below (6) is

$$|\psi_1\rangle = \frac{|0\rangle_0^{NS} + \alpha_{0;0}^\dagger |0\rangle_0^R}{\sqrt{2}}. \quad \text{(A8)}$$

As it will be useful, we will denote pair states in the NS sector by

$$|\bar{k}\rangle = |k \cup (-k)\rangle, \tag{A9}$$

with $k \subset \text{NS}_+$, and pair states in the R sector by

$$|\bar{\bar{k}}\rangle = |k \cup (-k) \cup \{0\}\rangle, \tag{A10}$$

with $k \subset \text{R}_+$.

2. Coherent states

Given a magnetic field h, a complex number A, and a function f, we define the so-called (fermionic) coherent states

$$\Psi_h^{\text{NS}}(A, f) = A \sum_{k \subset \text{NS}_+} \left[\prod_{k \in k} f(k) \right] |\bar{k}\rangle_h,$$

$$\Psi_h^{\text{R}}(A, f) = A \sum_{k \subset \text{R}_+} \left[\prod_{k \in k} f(k) \right] |\bar{\bar{k}}\rangle_h. \tag{A11}$$

The initial state $|\psi_1\rangle$ can be written as a sum of two coherent states in different sectors

$$|\psi_1\rangle = \frac{\Psi_0^{\text{NS}}(1, 0) + \Psi_0^{\text{R}}(1, 0)}{\sqrt{2}}. \tag{A12}$$

The crucial observation of our paper that allows us to derive the exact formulas given in Sec. II C is that a coherent state stays coherent if one changes the magnetic field h to another magnetic field $\tilde{h}$. Namely, we prove the following.

Lemma 1. Let $h, \tilde{h}$ be two arbitrary magnetic fields. We have

$$\Psi_h^{\text{NS}}(A, f) = \Psi_{\tilde{h}}^{\text{NS}}(\tilde{A}, \tilde{f}), \tag{A13}$$

with

$$\tilde{A} = A \prod_{k \in \text{NS}_+} \frac{1 + iK_{\tilde{h}h}(k)f(k)}{\sqrt{1 + K_{\tilde{h}h}^2(k)}} \tag{A14}$$

and

$$\tilde{f}(k) = \frac{iK_{\tilde{h}h}(k) + f(k)}{1 + iK_{\tilde{h}h}(k)f(k)}, \tag{A15}$$

where we defined

$$K_{\tilde{h}h}(k) = \tan \frac{\theta_k^{\tilde{h}} - \theta_k^h}{2}. \tag{A16}$$

We have an identical formula in the R sector.

Proof. We know the relations between the vacuum states at h and $\tilde{h}$, derived in [29],

$$|0\rangle_h^{\text{NS}} = \prod_{k \in \text{NS}_+} \left[\frac{1 + iK_{\tilde{h}h}(k)\alpha_{\tilde{h};-k}^\dagger \alpha_{\tilde{h};k}^\dagger}{\sqrt{1 + K_{\tilde{h}h}^2(k)}} \right] |0\rangle_{\tilde{h}}^{\text{NS}}, \tag{A17}$$

as well as the relations between creation operators at different magnetic fields

$$\alpha_{h;k} = \cos \frac{\theta_k^{\tilde{h}} - \theta_k^h}{2} \alpha_{\tilde{h},k} + i \sin \frac{\theta_k^{\tilde{h}} - \theta_k^h}{2} \alpha_{\tilde{h},-k}^\dagger. \tag{A18}$$

This allows us to write, for $r \subset \text{NS}_+$,

$$|\bar{r}\rangle_h = \frac{1}{\prod_{k \in \text{NS}_+} \sqrt{1 + K_{\tilde{h}h}^2(k)}} \prod_{r \in r} [iK_{\tilde{h}h}(r) + \alpha_{\tilde{h};-r}^\dagger \alpha_{\tilde{h};r}^\dagger]$$

$$\times \prod_{\substack{k \in \text{NS}_+ \\ k \notin r}} [1 + iK_{\tilde{h}h}(k)\alpha_{\tilde{h};-k}^\dagger \alpha_{\tilde{h};k}^\dagger] |0\rangle_{\tilde{h}}^{\text{NS}}. \tag{A19}$$

We deduce from this the formula for the overlaps between two pair states at different magnetic fields

$$_{\tilde{h}}\langle \bar{q} | \bar{r} \rangle_h = \frac{\prod_{k \in q \perp r} iK_{\tilde{h}h}(k)}{\prod_{k \in \text{NS}_+} \sqrt{1 + K_{\tilde{h}h}^2(k)}}, \tag{A20}$$

where $q \perp r = q \cup r - (q \cap r)$. The overlap between $|\bar{r}\rangle_h$ and $|q\rangle_h$ is zero if q is not a pair state. We now obtain

$$\Psi_h^{\text{NS}}(A, f) = \sum_{q \subset \text{NS}} |q\rangle_{\tilde{h}} {_{\tilde{h}}}\langle q | \Psi_h^{\text{NS}}(A, f) = A \sum_{q \subset \text{NS}_+} \sum_{r \subset \text{NS}_+} \left[\prod_{r \in r} f(r) \right] {_{\tilde{h}}}\langle \bar{q} | \bar{r} \rangle_h |\bar{q}\rangle_{\tilde{h}}$$

$$= \frac{A}{\prod_{k \in \text{NS}_+} \sqrt{1 + K_{\tilde{h}h}^2(k)}} \sum_{q \subset \text{NS}_+} \left[\prod_{q \in q} [iK_{\tilde{h}h}(q)] \sum_{r \subset \text{NS}_+} \prod_{r \in r} \times \begin{cases} \frac{f(r)}{iK_{\tilde{h}h}(r)} & \text{if } r \in q \\ iK_{\tilde{h}h}(r)f(r) & \text{if } r \notin q \end{cases} \right] |\bar{q}\rangle_{\tilde{h}}$$

$$= \frac{A}{\prod_{k \in \text{NS}_+} \sqrt{1 + K_{\tilde{h}h}^2(k)}} \sum_{q \subset \text{NS}_+} \left[\prod_{q \in q} [iK_{\tilde{h}h}(q)] \prod_{q \in q} \left(1 + \frac{f(q)}{iK_{\tilde{h}h}(q)} \right) \prod_{\substack{k \in \text{NS}_+ \\ k \notin q}} [1 + iK_{\tilde{h}h}(k)f(k)] \right] |\bar{q}\rangle_{\tilde{h}}$$

$$= \tilde{A} \sum_{q \subset \text{NS}_+} \left[\prod_{q \in q} \tilde{f}(q) \right] |\bar{q}\rangle_{\tilde{h}}, \tag{A21}$$

with $\tilde{A}, \tilde{f}$ defined in Lemma 1. $\blacksquare$

3. Energy and overlap

We note that the time evolution of a coherent state $\Psi_h^{\text{NS}}(A, f)$ with the Hamiltonian $H(h)$ is directly given by

$$e^{-itH(h)}\Psi_h^{\text{NS}}(A, f) = \Psi_h^{\text{NS}}(\tilde{A}, \tilde{f}), \quad \text{(A22)}$$

with

$$\tilde{f}(k) = e^{-2it\varepsilon_h(k)}f(k), \quad \tilde{A} = Ae^{-it\mathcal{E}^{\text{NS}}}, \quad \text{(A23)}$$

and $\mathcal{E}^{\text{NS}}$ the energy of the vacuum state $|0\rangle_h^{\text{NS}}$. A similar relation holds in the R sector. Thus, applying $2p$ times Lemma 1 successively with $h = \infty$ and $h = 0$, one finds

$$|\psi(\gamma, \beta)\rangle = \frac{\Psi_0^{\text{NS}}(A_{2p}^{\text{NS}}, f_{2p}) + \Psi_0^{\text{R}}(A_{2p}^{\text{R}}, f_{2p})}{\sqrt{2}}, \quad \text{(A24)}$$

with f_{2p} given by the recurrence (11) and $A_{2p}^{\text{NS,R}}$ by

$$A_{2p}^{\text{NS,R}} = \exp\left[-iL\left(\sum_{j=1}^{p}\beta_j + \gamma_j\right)\right]\prod_{j=0}^{2p-1}\prod_{k\in\text{NS,R}_+}$$

$$\times\left[\sin\frac{k}{2} + i(-1)^j\cos\frac{k}{2}f_j(k)\right]. \quad \text{(A25)}$$

In order to compute the expectation value of $H(h)$ of this state and the overlap with the ground state at magnetic field h, one performs another change of basis to h,

$$|\psi(\gamma, \beta)\rangle = \frac{\Psi_h^{\text{NS}}(A_{\text{proj}}^{\text{NS}}, f_{\text{proj}}) + \Psi_h^{\text{R}}(A_{\text{proj}}^{\text{R}}, f_{\text{proj}})}{\sqrt{2}}, \quad \text{(A26)}$$

with $f_{\text{proj}}(k)$ given in (12) and

$$A_{\text{proj}}^{\text{NS,R}} = A_{2p}^{\text{NS,R}}\prod_{k\in\text{NS,R}_+}\frac{1 + iK_{h0}(k)f_{2p}(k)}{\sqrt{1 + K_{h0}(k)^2}}. \quad \text{(A27)}$$

Under this form, the formula for the energy (14) is readily deduced. One also obtains the following formula for $\phi(h; \gamma, \beta)$, the overlap with the exact ground state:

$$\phi(h; \gamma, \beta) = \exp\left[-iL\left(\sum_{j=1}^{p}\beta_j + \gamma_j\right)\right]\frac{\phi^{\text{NS}}(h; \gamma, \beta)}{\sqrt{2}},$$

$$\phi^{\text{NS}}(h; \gamma, \beta) = \prod_{j=0}^{p-1}\prod_{k\in\text{NS}_+}\left[\sin\frac{k}{2} + i\cos\frac{k}{2}f_{2j}(k)\right]$$

$$\times\left[\sin\frac{k}{2} - i\cos\frac{k}{2}f_{2j+1}(k)\right]$$

$$\times\prod_{k\in\text{NS}_+}\frac{1 + iK_{h0}(k)f_{2p}(k)}{\sqrt{1 + K_{h0}^2(k)}}. \quad \text{(A28)}$$

One notes that the overlap with the spontaneously symmetry broken ground state is given by

$$\phi(h; \gamma, \beta) = \exp\left[-iL\left(\sum_{j=1}^{p}\beta_j + \gamma_j\right)\right]$$

$$\times\frac{\phi^{\text{NS}}(h; \gamma, \beta) + \phi^{\text{R}}(h; \gamma, \beta)}{2}, \quad \text{(A29)}$$

with ϕ^{R} defined similarly to ϕ^{NS} with products in R_+.

4. The X magnetization

The magnetization in the X direction is the simplest to determine, since X is local in terms of the fermions c_j. One first writes the state $|\psi(\gamma, \beta)\rangle$ as a sum of two coherent states at $h = \infty$. Using the Jordan-Wigner transformation (A2) and the Bogoliubov transformation (A4), one has

$$\langle X_i\rangle = 1 - \frac{2}{L}\sum_{k\in\text{NS}}\langle\alpha_{\infty;k}^\dagger\alpha_{\infty;k}\rangle, \quad \text{(A30)}$$

where $\langle\cdot\rangle$ denotes an expectation value in the coherent state $\Psi_\infty^{\text{NS}}(A, f)$. A similar formula holds in the R sector. Using then

$$\langle\alpha_{\infty;k}^\dagger\alpha_{\infty;k}\rangle = \frac{|f(k)|^2}{1 + |f(k)|^2}, \quad \text{(A31)}$$

one obtains the formula (15) in the thermodynamic limit. The formula (17) for the connected correlation of the magnetization in the X direction is obtained in a similar way.

5. The Z magnetization

The magnetization in the Z direction is more delicate, since Z is nonlocal in terms of the fermions. First, one notes that since the operator Z changes the sector, one has

$$m_Z(h; p) = \Re\left[\Psi_0^{\text{R}}(A_{2p}^{\text{R}}, f_{2p})^\dagger Z_j\Psi_0^{\text{NS}}(A_{2p}^{\text{NS}}, f_{2p})\right]$$

$$= \Re\left[(A_{2p}^{\text{R}})^*\sum_{q\subset\text{R}_+}\prod_{q\in q}[f_{2p}(q)^*]F(q)\right], \quad \text{(A32)}$$

with

$$F(q) = {}_0^{\text{R}}\langle\bar{q}|Z_j\Psi_0^{\text{NS}}(A_{2p}^{\text{NS}}, f_{2p}). \quad \text{(A33)}$$

Expressing $\Psi_0^{\text{NS}}(A_{2p}^{\text{NS}}, f_{2p})$ in terms of energy eigenstates, one obtains a sum over the full Hilbert space of matrix elements of the Z_j operator between two eigenstates, also called form factors. Their explicit expression is known and takes a particularly simple form at $h = 0$ [29,68–71],

$${}_0^{\text{R}}\langle q \cup \{0\}|Z_\ell|k\rangle_0^{\text{NS}}$$

$$= \exp\left[i\ell\left(\sum_{q\in q}q - \sum_{k\in k}k\right)\right]$$

$$\times\frac{(-i)^N}{L^N}\frac{\prod_{j<j'}\sin\frac{q_j-q_{j'}}{2}\prod_{j<j'}\sin\frac{k_j-k_{j'}}{2}}{\prod_{j,j'}\sin\frac{q_j-k_{j'}}{2}}, \quad \text{(A34)}$$

with N the number of elements of q and k. If this number differs in the two states then the form factor vanishes. In our case, the two states have to be pair states, and in this case one has the Cauchy determinant representation [38]

$${}_{\text{R}}\langle\bar{q}|Z_\ell|\bar{k}\rangle_{\text{NS}} = \frac{(-4)^N}{L^{2N}}(\det C)^2\prod_{j=1}^{N}\sin q_j\sin k_j, \quad \text{(A35)}$$

with N the number of elements of $q, k > 0$ and with the matrix

$$C_{ij} = \frac{1}{\cos q_i - \cos k_j}. \quad \text{(A36)}$$

Let us fix a $q \subset R_+$ with N particles. One has then

$$F(q) = \frac{A_{2p}^{NS}}{N!} \frac{(-4)^N}{L^{2N}}$$

$$\times \sum_{k_1,\dots,k_N \in NS_+} (\det C)^2 \prod_{j=1}^{N} [\sin q_j \sin k_j f_{2p}(k_j)]. \tag{A37}$$

We now prove the following lemma [38], using techniques introduced in [72].

Lemma 2. Given two functions $f(\lambda, \mu)$ and $g(\lambda, \mu)$, a set K, and two sets of numbers $\{\lambda_i\}_{i=1}^N$, $\{\mu_j\}_{j=1}^N$, we have the relation

$$\sum_{k_1,\dots,k_N \in K} \det_{i,j}[f(\lambda_i, k_j)] \det_{i,j}[g(k_i, \mu_j)]$$

$$= N! \det_{i,j} \left[\sum_{k \in K} f(\lambda_i, k) g(k, \mu_j) \right]. \tag{A38}$$

Proof. We write

$$\det_{i,j}[f(\lambda_i, k_j)] \det_{i,j}[g(k_i, \mu_j)] = \det_{i,j} \left[\sum_{s=1}^{N} f(\lambda_i, k_s) g(k_s, \mu_j) \right]$$

$$= \sum_{\sigma \in \mathfrak{S}_N} (-1)^\sigma C'_{1\sigma(1)} \cdots C'_{N\sigma(N)}, \tag{A39}$$

with $C'_{ij} = \sum_{s=1}^{N} f(\lambda_i, k_s) g(k_s, \mu_j)$. Then

$$\det_{i,j}[f(\lambda_i, k_j)] \det_{i,j}[g(k_i, \mu_j)]$$

$$= \sum_{s_1,\dots,s_N \in \{1,\dots,N\}} \sum_{\sigma \in \mathfrak{S}_N} (-1)^\sigma f(\lambda_1, k_{s_1}) g(k_{s_1}, \mu_{\sigma(1)})$$

$$\cdots f(\lambda_N, k_{s_N}) g(k_{s_N}, \mu_{\sigma(N)}). \tag{A40}$$

Now, if $s_i = s_j$, changing σ into $\sigma(ij)$ exactly multiplies the summand by -1, which makes this contribution vanish. Hence

$$\det_{i,j}[f(\lambda_i, k_j)] \det_{i,j}[g(k_i, \mu_j)]$$

$$= \sum_{\tau \in \mathfrak{S}_N} \sum_{\sigma \in \mathfrak{S}_N} (-1)^\sigma f(\lambda_1, k_{\tau(1)}) g(k_{\tau(1)}, \mu_{\sigma(1)})$$

$$\cdots f(\lambda_N, k_{\tau(N)}) g(k_{\tau(N)}, \mu_{\sigma(N)}). \tag{A41}$$

One can now perform the sum over $k_1, \dots, k_N$. The result is independent of τ, which gives the $N!$ in the lemma and the determinant formula. ∎

Using Lemma 2, we obtain

$$F(q) = A_{2p}^{NS} \det B, \tag{A42}$$

with

$$B_{ij} = \frac{4}{L^2} \sum_{k \in NS_+} \frac{\sin q_i f_{2p}(k) \sin k}{(\cos q_i - \cos k)(\cos q_j - \cos k)}. \tag{A43}$$

In our case, $f_{2p}(k)$ obtained from (11) is a regular function of k. Hence, in the thermodynamic limit $L \to \infty$ we obtain (see

[38])

$$B_{ij} = f_{2p}(q_i)\delta_{ij} - \frac{2\sin q_i}{\pi L(\cos q_i - \cos q_j)}$$

$$\times \left[\int_0^\pi \frac{f_{2p}(k)\sin k}{\cos q_i - \cos k} dk - \int_0^\pi \frac{f_{2p}(k)\sin k}{\cos q_j - \cos k} dk \right]$$

$$+ \mathcal{O}(L^{-2}). \tag{A44}$$

If $i = j$ the second term is understood as being the derivative obtained when $q_i \to q_j$.

Let us denote by $\rho(q)$ the so-called root density of q when $L \to \infty$, namely, the function such that $\rho(q)dqL$ is the number of elements in q between q and $q + dq$. It follows that one has the Fredholm determinant formula

$$F(q) = A_{2p}^{NS} \prod_{q \in q} [f_{2p}(q)] \det [\mathrm{Id} - J[\rho]][1 + \mathcal{O}(L^{-1})], \tag{A45}$$

with

$$J[\rho](\lambda, \mu) = \frac{2}{\pi} \frac{\rho(\lambda)\sin\lambda}{f_{2p}(\lambda)} \frac{1}{\cos\lambda - \cos\mu}$$

$$\times \int_0^\pi \left[\frac{f_{2p}(k)\sin k}{\cos\lambda - \cos k} - \frac{f_{2p}(k)\sin k}{\cos\mu - \cos k} \right] dk. \tag{A46}$$

We now return to (A32), which is a weighted sum of the root-density-dependent quantity $\det [\mathrm{Id} - J[\rho]]$ over all the eigenstates. We have the following lemma, using ideas of [73].

Lemma 3. Let $F[q]$ be a function of q and $f(k)$ a function. We define

$$\langle F \rangle = \frac{1}{\prod_{k \in NS_+} [1 + |f(k)|^2]} \sum_{q \subset NS_+} F[q] \prod_{q \in q} [|f(q)|^2]. \tag{A47}$$

If $F[q] = F[\rho]$ depends only on the root density ρ of q in the thermodynamic limit, then

$$\langle F \rangle = F[\rho_s] + o(L^0), \tag{A48}$$

with

$$\rho_s(k) = \frac{1}{2\pi} \frac{|f(k)|^2}{1 + |f(k)|^2}. \tag{A49}$$

Proof. Let us first treat the particular case where in the thermodynamic limit F depends only on r, the number of elements of q divided by L. We introduce the generating function

$$\Gamma(\alpha) = \frac{1}{\prod_{k \in NS_+} [1 + |f(k)|^2]} \sum_{q \subset NS_+} \prod_{q \in q} \left[\left(1 + \frac{\alpha}{L} \right) |f(q)|^2 \right]. \tag{A50}$$

By differentiating with respect to α, we see that

$$\langle r^j \rangle = \Gamma^{(j)}(0) + \mathcal{O}(L^{-1}). \tag{A51}$$

In addition, performing the summation on q, we obtain

$$\Gamma(\alpha) = \prod_{k \in NS_+} \left[1 + \frac{\alpha}{L} \frac{|f(k)|^2}{1 + |f(k)|^2} \right]. \tag{A52}$$

From this we find, for any j,

$$\langle r^j \rangle = \left(\int_0^\pi \rho_s(k) dk \right)^j + \mathcal{O}(L^{-1}). \quad (A53)$$

As any regular function on $[0, \pi]$ can be approximated by a polynomial with arbitrary precision provided its degree is high enough, this establishes the result of the lemma when F is a function of r only.

Let us now divide $[0, \pi]$ into m windows $W_k = [\frac{\pi}{m}(k-1), \frac{\pi}{m}k]$ for $k = 1, \ldots, m$ and consider $F[r_1, \ldots, r_m]$ a function of q that in the thermodynamic limit depends only on r_k, the number of elements of q in W_k divided by L. By introducing $\Gamma(\alpha_1, \ldots, \alpha_m)$ as in (A50) with α replaced by α_k where k is such that $q \in W_k$, we get similarly

$$\langle r_1^{j_1} \cdots r_m^{j_m} \rangle = \left(\int_{W_1} \rho_s \right)^{j_1} \cdots \left(\int_{W_m} \rho_s \right)^{j_m} + \mathcal{O}(L^{-1}). \quad (A54)$$

Hence the lemma holds whenever F is a function of $r_1, \ldots, r_m$ only. Since any regular functional of ρ can be approximated with arbitrary precision by such a function F provided m is large enough, the lemma holds for general $F[\rho]$. ∎

Using (A45) in (A32) and Lemma 3, one obtains the formula (18) for the Z magnetization in the thermodynamic limit.

APPENDIX B: COHERENT GATES

In this Appendix we show that $\exp(it \sum_{j=1}^L Y_j Y_{j+1})$ gates can be incorporated in the quantum circuit considered in this paper, while still staying exactly solvable.

1. Change of Pauli matrices

Given a set of Pauli matrices X, Y, Z, the operators defined by the rotation

$$X' = -X, \quad Y' = Z, \quad Z' = Y \quad (B1)$$

give another set of Pauli matrices. The Ising Hamiltonian becomes

$$H(h) = -\sum_{j=1}^L Y_j' Y_{j+1}' - h X_j'. \quad (B2)$$

Performing a Jordan-Wigner transformation as in (A2) with fermions c_j', one finds the relation

$$c_j' = i(-1)^j c_j^\dagger, \quad (B3)$$

which results in

$$c'(k) = ic(\pi - k)^\dagger. \quad (B4)$$

This results in the following relation for the corresponding $\alpha_{h;k}'$ in (A4),

$$\alpha_{-\infty;-k}' = -\text{sgn}(k)\alpha_{\infty;\pi-k}. \quad (B5)$$

We deduce that the coherent states $\Psi_h^{\text{NS,R}'}(A, f)$ built from these new fermions satisfy

$$\Psi_\infty^{\text{NS}}(A, f) = \Psi_{-\infty}^{\text{NS}'}(A, \tilde{f}), \quad (B6)$$

with

$$\tilde{f}(k) = f(\pi - k). \quad (B7)$$

An identical transformation holds in the R sector. By using Lemma A, one can thus transform a coherent state at magnetic field h in the original set of Pauli matrices into another coherent state at magnetic field $\tilde{h}$ in the new set of Pauli matrices. In particular, at $h = 0$, this allows us to apply a $\exp(it \sum_{j=1}^L Y_j Y_{j+1})$ gate to the state of the model.

2. Set of coherent gates

We obtain that the state of the quantum computer is exactly tractable whenever it is initialized in a superposition of coherent states (A11) and time evolved with the gates $\exp(it \sum_{j=1}^L X_j)$, $\exp(it \sum_{j=1}^L Y_j Y_{j+1})$, or $\exp(it \sum_{j=1}^L Z_j Z_{j+1})$ in any order. We call this set of gates coherent gates since they all map a coherent state onto a coherent state.

To present the transformation rules, without loss of generality one can assume by linearity that it is initialized in a unique coherent state, and since Lemma A shows that all magnetic fields h are equivalent, one can assume that this coherent state is prepared with $h = \infty$. Hence we assume it is initialized in

$$|\psi\rangle = \Psi_\infty^{\text{NS}}(A, f), \quad (B8)$$

with A a complex number and f a function on $[0, \pi]$. Under the application of any coherent gates, the state stays coherent but its parameters are changed

$$\exp\left(it \sum_{j=1}^L \Gamma_j \right) |\psi\rangle = \Psi_\infty^{\text{NS}}(\tilde{A}, \tilde{f}), \quad (B9)$$

with

$$\tilde{f}(k) = e^{-4it} f(k) \quad \text{if } \Gamma_j = X_j,$$

$$\tilde{f}(k) = \frac{-i\tan(k/2)(1 - e^{-4it}) + [1 + \tan^2(k/2)e^{-4it}]f(k)}{\tan^2(k/2) + e^{-4it} + i\tan(k/2)(1 - e^{-4it})f(k)} \quad \text{if } \Gamma_j = Y_j Y_{j+1}, \quad (B10)$$

$$\tilde{f}(k) = \frac{i\tan(k/2)(1 - e^{-4it}) + [1 + \tan^2(k/2)e^{-4it}]f(k)}{\tan^2(k/2) + e^{-4it} - i\tan(k/2)(1 - e^{-4it})f(k)} \quad \text{if } \Gamma_j = Z_j Z_{j+1}.$$

APPENDIX C: THE Z MAGNETIZATION AFTER A QUANTUM QUENCH

In this Appendix we show how the techniques developed in this paper can be applied to quantum quenches in the Ising model [26–38]. This problem consists in initializing the state of the system $|\psi(t)\rangle$ in the ground state of $H(h_0)$ at magnetic field h_0 and time evolving it at $t > 0$ with the Hamiltonian $H(h)$ at another magnetic field h.

Using (A17) derived in [29], one finds that the time-evolved state is

$$|\psi(t)\rangle = \frac{\Psi_h^{\mathrm{NS}}(A^{\mathrm{NS}}, f_t) + \Psi_h^{\mathrm{R}}(A^{\mathrm{R}}, f_t)}{\sqrt{2}}, \qquad (C1)$$

with

$$A^{\mathrm{NS,R}} = \frac{1}{\prod_{k \in \mathrm{NS,R}_+} \sqrt{1 + K_{hh_0}^2(k)}},$$

$$f_t(k) = iK_{hh_0}(k)e^{-2it\varepsilon_h(k)}. \qquad (C2)$$

The difficulty encountered before is that the form factors of Z_j between eigenstates of $H(h)$ are rather complicated [29,68–71] and do not allow for a resummation of the one-point function of Z_j when expressed as a spectral sum. The idea is thus to perform a change of basis to $h = 0$, with Lemma 1,

$$|\psi(t)\rangle = \frac{\Psi_0^{\mathrm{NS}}(\tilde{A}^{\mathrm{NS}}, \tilde{f}_t) + \Psi_0^{\mathrm{R}}(\tilde{A}^{\mathrm{R}}, \tilde{f}_t)}{\sqrt{2}}, \qquad (C3)$$

with

$$\tilde{A}_t^{\mathrm{NS,R}} = A^{\mathrm{NS,R}} \prod_{k \in \mathrm{NS,R}_+} \frac{1 + iK_{0h}(k)f_t(k)}{\sqrt{1 + K_{0h}^2(k)}},$$

$$\tilde{f}_t(k) = \frac{iK_{0h}(k) + f_t(k)}{1 + iK_{0h}(k)f_t(k)}. \qquad (C4)$$

Then one obtains exactly the formula (18) for the Z magnetization after the quench, with f_{2p} replaced by $\tilde{f}_t$.

[1] J. Preskill, Quantum computing in the NISQ era and beyond, Quantum **2**, 79 (2018).

[2] F. Arute *et al.*, Quantum supremacy using a programmable superconducting processor, Nature (London) **574**, 505 (2019).

[3] H.-S. Zhong *et al.*, Quantum computational advantage using photons, Science **370**, 1460 (2020).

[4] R. Blatt and C. F. Ross, Quantum simulations with trapped ions, Nat. Phys. **8**, 277 (2012).

[5] J. Zhang, G. Pagano, P. W. Hess, A. Kyprianidis, P. Becker, H. Kaplan, A. V. Gorshkov, Z.-X. Gong, and C. Monroe, Observation of a many-body dynamical phase transition with a 53-qubit quantum simulator, Nature (London) **551**, 601 (2017).

[6] R. Islam, C. Senko, W. C. Campbell, S. Korenblit, J. Smith, A. Lee, E. E. Edwards, C.-C. J. Wang, J. K. Freericks, and C. Monroe, Emergence and frustration of magnetism with variable-range interactions in a quantum simulator, Science **340**, 583 (2013).

[7] R. Islam, R. Ma, P. M. Preiss, M. E. Tai, A. Lukin, M. Rispoli, and M. Greiner, Measuring entanglement entropy in a quantum many-body system, Nature (London) **528**, 77 (2015).

[8] M. Greiner, O. Mandel, T. Esslinger, T. W. Hänsch, and I. Bloch, Quantum phase transition from a superfluid to a Mott insulator in a gas of ultracold atoms, Nature (London) **415**, 39 (2002).

[9] I. Bloch, J. Dalibard, and W. Zwerger, Many-body physics with ultracold gases, Rev. Mod. Phys. **80**, 885 (2008).

[10] H. Bernien *et al.*, Probing many-body dynamics on a 51-atom quantum simulator, Nature (London) **551**, 579 (2017).

[11] J. I. Cirac and P. Zoller, Goals and opportunities in quantum simulation, Nat. Phys. **8**, 264 (2012).

[12] M. Aidelsburger, M. Atala, M. Lohse, J. T. Barreiro, B. Paredes and I. Bloch, Realization of the Hofstadter Hamiltonian with Ultracold Atoms in Optical Lattices, Phys. Rev. Lett. **111**, 185301 (2013).

[13] S. Choi *et al.*, Observation of discrete time-crystalline order in a disordered dipolar many-body system, Nature (London) **543**, 221 (2017).

[14] M. Aidelsburger, M. Lohse, C. Schweizer, M. Atala, J. T. Barreiro, S. Nascimbène, N. R. Cooper, I. Bloch, and N. Goldman, Measuring the Chern number of Hofstadter bands with ultracold bosonic atoms, Nat. Phys. **11**, 162 (2015).

[15] J.-Y. Choi, S. Hild, J. Zeiher, P. Schauss, A. Rubio-Abadal, T. Yefsah, V. Khemani, D. A. Huse, I. Bloch, and C. Gross, Exploring the many-body localization transition in two dimensions, Science **352**, 1547 (2016).

[16] R. P. Feynman, Simulating physics with computers, Int. J. Theor. Phys. **21**, 467 (1982).

[17] M. E. Fisher and M. N. Barber, Scaling Theory for Finite-Size Effects in the Critical Region, Phys. Rev. Lett. **28**, 1516 (1972).

[18] E. Brézin, An investigation of finite size scaling, J. Phys. (Paris) **43**, 15 (1982).

[19] J. Cardy, *Finite-Size Scaling* (North-Holland, Amsterdam, 1988), Vol. 2.

[20] J. Um, S.-I. Lee, and B. J. Kim, Quantum phase transition and finite-size scaling of the one-dimensional Ising model, J. Korean Phys. Soc. **50**, 285 (2007).

[21] B. Vanhecke, J. Haegeman, K. van Acoleyen, L. Vanderstraeten, and F. Verstraete, A Scaling Hypothesis for Matrix Product States, Phys. Rev. Lett. **123**, 250604 (2019).

[22] W. W. Ho and T. H. Hsieh, Efficient variational simulation of non-trivial quantum states, SciPost Phys. **6**, 029 (2019).

[23] E. Farhi, J. Goldstone, and S. Gutmann, A quantum approximate optimization algorithm, arXiv:1411.4028.

[24] E. Farhi and A. W. Harrow, Quantum supremacy through the quantum approximate optimization algorithm, arXiv:1602.07674

[25] L. Onsager, Crystal statistics. I. A two-dimensional model with an order-disorder transition, Phys. Rev. **65**, 117 (1944).

[26] K. Sengupta, S. Powell, and S. Sachdev, Quench dynamics across quantum critical points, Phys. Rev. A **69**, 053616 (2004).

[27] D. Rossini, A. Silva, G. Mussardo, and G. E. Santoro, Effective Thermal Dynamics Following a Quantum Quench in a Spin Chain, Phys. Rev. Lett. **102**, 127204 (2009).

[28] P. Calabrese, F. H. L. Essler, and M. Fagotti, Quantum Quench in the Transverse-Field Ising Chain, Phys. Rev. Lett. **106**, 227203 (2011).

[29] P. Calabrese, F. H. L. Essler, and M. Fagotti, Quantum quench in the transverse field Ising chain I: Time evolution of order parameter correlators, J. Stat. Mech. (2012) P07016.

[30] L. Foini, L. F. Cugliandolo, and A. Gambassi, Dynamic correlations, fluctuation-dissipation relations, and effective temperatures after a quantum quench of the transverse field Ising chain, J. Stat. Mech. (2012) P09011.

[31] B. Blass, H. Rieger, and F. Iglòi, Quantum relaxation and finite-size effects in the XY chain in a transverse field after global quenches, Europhys. Lett. **99**, 30004 (2012).

[32] D. Schuricht and F. H. L. Essler, Dynamics in the Ising field theory after a quantum quench, J. Stat. Mech. (2012) P04017.

[33] F. Iglói and H. Rieger, Quantum Relaxation after a Quench in Systems with Boundaries, Phys. Rev. Lett. **106**, 035701 (2011).

[34] H. Rieger and F. Iglói, Semiclassical theory for quantum quenches in finite transverse Ising chains, Phys. Rev. B **84**, 165117 (2011).

[35] M. Fagotti and F. H. L. Essler, Quench dynamics and relaxation in isolated integrable quantum spin chains, J. Stat. Mech. (2016) 064002.

[36] G. Delfino and J. Viti, On the theory of quantum quenches in near-critical systems, J. Phys. A: Math. Theor. **50**, 084004 (2017).

[37] M. Collura, Relaxation of the order-parameter statistics in the Ising quantum chain, SciPost Phys. **7**, 072 (2019).

[38] E. Granet, M. Fagotti, and F. H. L. Essler, Finite temperature and quench dynamics in the transverse field Ising model from form factor expansions, SciPost Phys. **9**, 033 (2020).

[39] H. W. J. Blöte, J. L. Cardy, and M. P. Nightingale, Conformal Invariance, the Central Charge, and Universal Finite-Size Amplitudes at Criticality, Phys. Rev. Lett. **56**, 742 (1986).

[40] I. Affleck, Universal Term in the Free Energy at a Critical Point and the Conformal Anomaly, Phys. Rev. Lett. **56**, 746 (1986).

[41] C. Itzykson, H. Saleur, and J.-B. Zuber, *Conformal Invariance and Applications to Statistical Mechanics* (World Scientific, Singapore, 1998).

[42] W. van Dam, M. Mosca, and U. Vazirani, Proceedings of the 42nd IEEE Symposium on Foundations of Computer Science, Las Vegas, 2001 (IEEE Computer Society, Los Alamitos, 2001).

[43] C. J. Hamer and M. Barber, Finite-size scaling and quantum Hamiltonian field theory: The transverse Ising model, INIS IAEA Report No. UM-P-79/21, 1979 (unpublished).

[44] P. Pfeuty, The one-dimensional Ising model with a transverse field, Ann. Phys. (NY) **57**, 79 (1970).

[45] A. Sorge, pyfssa 0.7.6, Zenodo: A scientific Python package for finite-size scaling analysis (CERN, Meyrin, 2015), available at https://zenodo.org/record/35293#.YYNonC2ZPEY.

[46] S. Wang, E. Fontana, M. Cerezo, K. Sharma, A. Sone, L. Cincio, and P. J. Coles, A variational eigenvalue solver on a quantum processor, Nat. Commun. **5**, 4213 (2014).

[47] B. F. Schiffer, J. Tura, and J. I. Cirac, Adiabatic spectroscopy and a variational quantum adiabatic algorithm, arXiv:2103.01226.

[48] B. Bauer, S. Bravyi, M. Motta, and G. K.-L. Chan, Quantum algorithms for quantum chemistry and quantum materials science, Chem. Rev. **120**, 12685 (2020).

[49] M. Cerezo, A. Arrasmith, R. Babbush, S. C. Benjamin, S. Endo, K. Fujii, J. R. McClean, K. Mitarai, X. Yuan, L. Cincio, and P. J. Coles, Variational quantum algorithms, Nat. Rev. Phys. **3**, 625 (2021).

[50] K. Bharti, A. Cervera-Lierta, T. H. Kyaw, T. Haug, S. Alperin-Lea, A. Anand, M. Degroote, H. Heimonen, J. S. Kottmann, T. Menke, W.-K. Mok, S. Sim, L.-C. Kwek, and A. Aspuru-Guzik, Noisy intermediate-scale quantum (NISQ) algorithms, arXiv:2101.08448.

[51] S. Endo, Z. Cai, S. C. Benjamin, and X. Yuan, Hybrid quantum-classical algorithms and quantum error mitigation, J. Phys. Soc. Jpn. **90**, 032001 (2021).

[52] L. Bassman, M. Urbanek, M. Metcalf, J. Carter, A. F. Kemper, and W. de Jong, Simulating quantum materials with digital quantum computers, Quantum Sci. Technol. **6**, 043002 (2021).

[53] G. Greene-Diniz and D. M. Ramo, Generalized unitary coupled cluster excitations for multireference molecular states optimized by the variational quantum eigensolver, arXiv:1910.05168.

[54] H. R. Grimsley, S. E. Economou, E. Barnes, and N. J. Mayhall An adaptive variational algorithm for exact molecular simulations on a quantum computer, Nat. Commun. **10**, 3007 (2019).

[55] J. Lee, W. J. Huggins, M. Head-Gordon, and K. B. Whaley, Generalized unitary coupled cluster wavefunctions for quantum computation, J. Chem. Theory Comput. **15**, 311 (2019).

[56] S. McArdle, S. Endo, A. Aspuru-Guzik, S. C. Benjamin, and X. Yuan, Quantum computational chemistry, Rev. Mod. Phys. **92**, 015003 (2020).

[57] J. I. Colless, V. V. Ramasesh, D. Dahlen, M. S. Blok, M. E. Kimchi-Schwartz, J. R. McClean, J. Carter, W. A. de Jong, and I. Siddiqi, Computation of Molecular Spectra on a Quantum Processor with an Error-Resilient Algorithm, Phys. Rev. X **8**, 011021 (2018).

[58] O. Higgott, D. Wang, and S. Brierley, Variational quantum computation of excited states, Quantum **3**, 156 (2019).

[59] K. M. Nakanishi, K. Mitarai, and K. Fujii, Subspace-search variational quantum eigensolver for excited states, Phys. Rev. Res. **1**, 033062 (2019).

[60] T. E. O'Brien, B. Senjean, R. Sagastizabal, X. Bonet-Monroig, A. Dutkiewicz, F. Buda, L. DiCarlo, and L. Visscher, Calculating energy derivatives for quantum chemistry on a quantum computer, npj Quantum Inf. **5**, 113 (2019).

[61] S. McArdle, T. Jones, S. Endo, Y. Li, S. C. Benjamin, and X. Yuan, Variational ansatz-based quantum simulation of imaginary time evolution, npj Quantum Inf. **5**, 75 (2019).

[62] M. Motta, C. Sun, A. T. K. Tan, M. J. O'Rourke, E. Ye, A. J. Minnich, F. G. S. L. Brandão, and G. K.-L. Chan, Determining eigenstates and thermal states on a quantum computer using quantum imaginary time evolution, Nat. Phys. **16**, 205 (2020).

[63] D. Z. Manrique, I. T. Khan, K. Yamamoto, V. Wichitwechkarn, and D. Muñoz Ramo, Momentum-space unitary coupled cluster and translational quantum subspace expansion for periodic systems on quantum computers, arXiv:2008.08694.

[64] I. Rungger, N. Fitzpatrick, H. Chen, C. H. Alderete, H. Apel, A. Cowtan, A. Patterson, D. Muñoz Ramo, Y. Zhu, N. H. Nguyen, E. Grant, S. Chretien, L. Wossnig, N. M. Linke, and R. Duncan, Dynamical mean field theory algorithm and experiment on quantum computers, arXiv:1910.04735.

[65] N. Yoshioka, Y. O. Nakagawa, Y.-Y. Ohnishi, and W. Mizukami, Variational quantum simulation for periodic materials, arXiv:2008.09492.

[66] J. Liu, L. Wan, Z. Li, and J. Yang, Simulating periodic systems on quantum computer, arXiv:2008.02946.

[67] S. Wang, E. Fontana, M. Cerezo, K. Sharma, A. Sone, L. Cincio, and P. J. Coles, Noise-induced barren plateaus in variational quantum algorithms, Nat. Commun. **12**, 6961 (2021).

[68] A. Bugrij, Correlation function of the two-dimensional Ising model on the finite lattice. I, Theor. Math. Phys. **127**, 528 (2001).

[69] A. Bugrij and O. Lisovyy, Spin matrix elements in 2D Ising model on the finite lattice, Phys. Lett. A **319**, 390 (2003).

[70] G. von Gehlen, N. Iorgov, S. Pakuliak, V. Shadura, and Y. Tykhyy, Form-factors in the Baxter-Bazhanov-Stroganov model II: Ising model on the finite lattice, J. Phys. A: Math. Theor. **41**, 095003 (2008).

[71] N. Iorgov, V. Shadura, and Y. Tykhyy, Spin operator matrix elements in the quantum Ising chain: Fermion approach, J. Stat. Mech. (2011) P02028.

[72] V. E. Korepin and N. A. Slavnov, The time dependent correlation function of an impenetrable Bose gas as a Fredholm minor. I, Commun. Math. Phys. **129**, 103 (1990).

[73] J.-S. Caux and F. H. L. Essler, Time Evolution of Local Observables after Quenching to an Integrable Model, Phys. Rev. Lett. **110**, 257203 (2013).